51 p.

UNPUBLISHED PRELIMINARY DATA

N64-15386 *

CODE-1

(NASA CR-55542) OTS

# FERROELECTRIC BOLOMETER FOR SPACE RESEARCH *

OTS PRICE

XEROX $ 5.60 ph.

MICROFILM $ 1.91 mf.

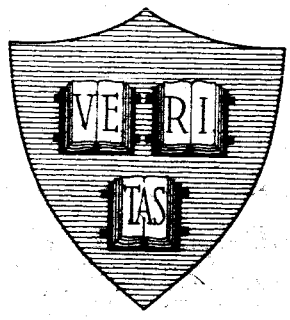


by

HECTOR C. INGRAO, FREDERICK J. KAHN, AND DONALD H. MENZEL

HARVARD COLLEGE OBSERVATORY

CAMBRIDGE, MASS., U.S.A.

3932001

* SCIENTIFIC REPORT No. 3

NASA RESEARCH GRANT No. NsG 64-60

NOVEMBER 1, 1963

PREPARED FOR

NATIONAL AERONAUTICS AND SPACE ADMINISTRATION

# FERROELECTRIC BOLOMETER FOR SPACE RESEARCH

by

Hector C. Ingrao, Frederic J. Kahn, and Donald H. Menzel

Harvard College Observatory
Cambridge, Massachusetts (USA)

Scientific Report No. 3

NASA RESEARCH GRANT No. NsG 64-60

* * * * *

November 1, 1963

Prepared for

NATIONAL AERONAUTICS AND SPACE ADMINISTRATION

## ABSTRACT

# FERROELECTRIC BOLOMETER FOR SPACE RESEARCH

by

Hector C. Ingrao, Frederic J. Kahn*, and Donald H. Menzel

Harvard College Observatory
Cambridge, Massachusetts (USA)

15386

In this report we compare the ferroelectric bolometer with other thermal detectors for use in space instrumentation.

We manufactured ceramic ferroelectric bolometers with Curie points between $-10^{o}C$ and $+10^{o}C$ and dimensions as low as .5 mm x .5 mm x 50 microns. We measured the performance of a radiation pyrometer with a ferroelectric bolometer 1.0 mm x 1.0 mm x 0.2 mm. With an incident infrared signal of $5.8 \times 10^{-9}$ watts peak-to-peak, chopped at 2.5 cps, and a bandpass $\Delta f = 0.25$ cps, at room temperature, the noise level of the system is $4.2 \times 10^{-10}$ watts rms. Theoretical analyses of the responsivity and minimum detectable power are presented. Work sponsored by the National Aeronautics and Space Administration.

AUTHOR


---


*Present address: Division of Engineering and Applied Physics, Harvard University, Cambridge, Massachusetts (USA).

TABLE OF CONTENTS


| | Page |
|---|---|
| Introduction | 1 |
| Response Analysis | 7 |
| Experimental Results | 31 |
| Noise Analysis | 34 |
| Improvement of Responsivity | 40 |
| Acknowledgments | 42 |
| Bibliography | 43 |

# INTRODUCTION

There exist in space research many observational problems for which solutions can be found in the 7μ - 40μ region of the electromagnetic spectrum. Temperature measurements of planetary surfaces and atmosphere, infrared planetary albedo, etc., can be counted among the aspects of high scientific interest that we can explore in the 7μ - 40μ band.

The 8μ - 14μ region is of special interest since this region is a broad atmospheric window which permits observation from ground-base stations or from space vehicles, with the same type of instrument. This is particularly advantageous, for example, for measuring lunar temperatures in the same area simultaneously from a space craft close to the Moon and from similar equipment on the ground.

After the experiment has been designed, an evaluation of the signal levels and the signal to noise ratios for a certain bandpass will indicate the maximum noise level that can be tolerated in the system. In experiments where it is possible to use single detectors, these detectors will fall into two main categories: quantum or thermal type.[1] In the quantum group we find detectors using the photoconductive, photovoltaic and photoelectromagnetic (pem) effects. For these detectors to operate at wave lengths in the region of our interest (8μ - 14μ), they must be used with cryogenic devices. A

possible exception in this category might be a detector using a mechanism discovered by Diemer.[2*] At present, however, a working detector based on this principle is not available.[3]

In the category of single thermal detectors are thermocouples, thermopiles, bolometers of different kinds, pneumatic detectors, and detectors that use differences in thermal linear expansion.

Analysis of the performance of this group shows that, of commercially available detectors, the one best suited to space instrumentation is the thermistor bolometer. This detector satisfies the requirement of relatively low NEP, can be obtained in small sizes and different shapes, tolerates the vibration encountered during the launching of a space craft, has a time constant of the order of milliseconds, and a reasonable electrical impedance. For example, we have in operation a Germanium-immersed thermistor bolometer, 0.1 mm x 0.1 mm in size, with a time constant of 5 milliseconds and a NEP of $5 \times 10^{-11}$ watts per 1 cps bandpass. As one might expect, this detector has certain drawbacks too. Since the resistance of the bolometer operating at room temperature is

---

*In contrast to all other quantum infrared detectors the principle of operation of the proposed detector does not involve free carrier generation by the infrared radiation. Instead the detector will use the absorption of infrared energy by excitons to quench an exciton--induced photo-conductivity.

about $10^6$ ohms and the corresponding bias about 50 volts, the power dissipated in the detector is about $2.5 \times 10^{-3}$ watts. Since the detector has a negative coefficient, increase in the ambient temperature will reduce the resistance. Hence there will be a risk of reaching a runaway point resulting in the self-destruction of the detector. Usually the operating bias is set at 60% of the runaway voltage.[4] The irreducible noise in the thermistor is Johnson and current noise, and is well above the signal originated by the thermal statistical fluctuations in the detector itself, the irreducible noise in an ideal thermal detector.

The ferroelectric bolometer can operate in two modes. The dielectric mode employs the charge of induced polarization with temperature. The pyroelectric mode makes use of the charge of spontaneous polarization. As we will show, under certain conditions the ferroelectric bolometer is close to being an ideal thermal detector. Furthermore, it can operate satisfactorily over a wide temperature range with bias from a constant voltage source. The problem of damage to the detector over a wide range in temperature (of the order of several hundred degrees centigrade) does not exist.

Since the internal dc resistance is approximately $10^{12}\,\Omega$, the power dissipated by the bias in the detector will be approximately $10^{-8}$ watts. For a typical bias of 100 volts this is a factor of $10^5$ less than in the thermistor bolometer. The other important characteristic is that under certain

operating conditions the signal output is proportional to the derivative of the temperature in the detector with respect to time. Thus, it is possible to use this characteristic as a redundancy discriminator for a scanning system. Moreover, if the detector operates in the pyroelectric mode, no external power supply for biasing is required.

Planetary problems lead us to investigate different schemes of image forming systems. In the course of this work and as part of the effort to develop a thermal image-forming system of simultaneous read-in for lunar observations,[5] our laboratory has built and tested several single thermal detectors using the combined pyroelectric and dielectric variations of $(Ba,Sr)TiO_3$ solid solutions as a function of the temperature near the Curie point.[1, 6] Our current detectors are made of a $Ba(Ti,Sn)O_3$ with the addition of various impurities including rare earths. When we began our program in 1960, we did not know that other laboratories were engaged in work in this field. We have since learned that Burns[7] has analyzed the possibility of a thermal image tube that uses ferroelectric material as a target plate.

Hanel[8] has shown theoretically that under certain conditions a good single crystal of $BaTiO_3$ used as a temperature-sensitive capacitance can achieve temperature noise-limited operation. Cooper[9] has extended the analysis to the pyroelectric effect of $BaTiO_3$ single crystal and has

shown that under certain operating conditions the bolometer would be limited only by temperature fluctuations. Both of the above calculations make rather optimistic assumptions and use values for the thermal and electrical parameters of the detector material without analyzing the simultaneous pyroelectric and dielectric variations as a function of temperature for dc operation.

Mattes and Perals[10] have made a pyroelectric transducer of $BaTiO_3$ ceramic for measuring large temperature changes of tens of degrees. Lang,[11] reported that by using pyroelectric phenomena in a rod of $BaTiO_3$ ceramic he detected temperature changes of $2 \times 10^{-7}$°C. More recently the Boeing Company analyzed, theoretically and experimentally, ferroelectric bolometers in the pyroelectric and dielectric modes of operation. They used two different crystals, potassium dihydrogen phosphate (KDP) and triglycine sulphate (TGS). The KDP has a Curie point at 123°K and the TGS at 498°C.

The characteristics of the detectors are given in Table I. Boeing obtained best results with the TGS detector operating at a NEP of $8.1 \times 10^{-9}$ watts per 5 cps bandwidth.

We will find the analytical expressions that relate the responsivity, electrical, thermal time constants and minimum detectable power to the physical properties of the detector and its operating conditions.

TABLE I*

DATA OF EXPERIMENTAL FERROELECTRIC BOLOMETER AND PYROELECTRIC RECEIVERS FROM BOEING COMPANY, RENTON, WASHINGTON

| | | Detector | |
|---|---|---|---|
| | | KDP | TGS |
| Detector Area ($mm^2$) | | 25 | 25 |
| Detector Thickness (mm) | | 0.5 | 0.075 |
| Curie Point ($^oK$) | | 123 | 322.8 |
| Operating Temperature ($^oK$) | | 123.4 | 248 |
| Responsivity volt watt-1 | Computed | 439 | 254 |
| | Measured | 250 | 274 |
| NEP** | Computed | $2.69 \times 10^{-9}$ | $2.37 \times 10^{-9}$ |
| | Measured | $3.8 \times 10^{-8}$ | $8.1 \times 10^{-9}$ |
| Thermal Time Constant (sec) | Computed | 90 | 102 |
| | Measured | 0.0084 | 0.0145 |

*Data from reference 12.

**The NEP is given in watts rms for a 5 cps bandpass.

We first consider the heat balance of the ferroelectric bolometer. The equivalent circuit of the detector operating at a temperature $T_o$ is given in Figure 1. The detector element is represented by capacitor $C_D$ in parallel with an equivalent leakage resistor $R_D$.

$E_{bb}$ is an external battery biasing the detector and $R_L$ is the real part of the input impedance of the electrometer used to measure the current output of the detector. The detector output (i) is measured as fluctuations in $I_L$. W is the infrared input to the detector.

Let $W_h$ be the power dissipated in the resistor $R_D$ due to the dc bias; $T_o$, the ambient temperature; w, the infrared signal. If T is the mean temperature of the detector, then

$$\mathcal{C} \frac{dT}{dt} + \mathcal{G} (T-T_o) = W_h + w \qquad (1)$$

where $\mathcal{C}$ is the equivalent thermal capacity of the detector, $\mathcal{G}$ is the equivalent thermal conductance due to both conduction and radiation, and we have assumed an emissivity of unity.

If $V_D$ is the detector bias, the joule heating will be

$$W_h = \frac{V_D^2}{R_D} \qquad (2)$$

Since the ferroelectric bolometer detects only changes in temperature, we now separate T and $W_h$ into constant and time varying components.

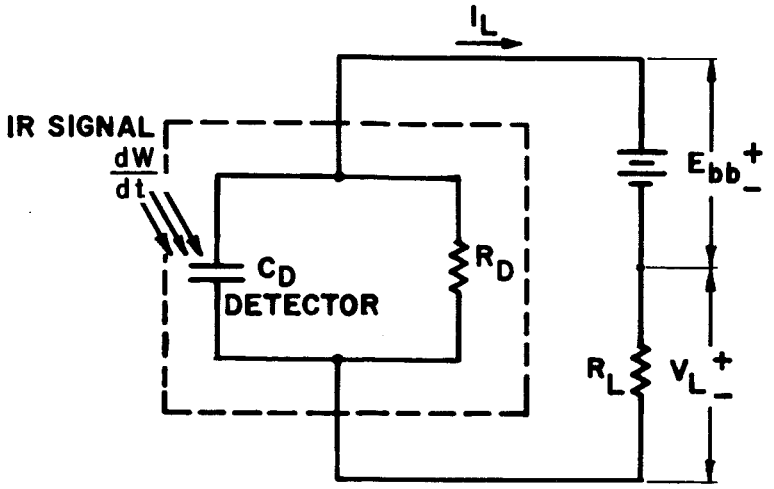


Fig. 1. Equivalent circuit of ferroelectric bolometer. $C_D$ = capacitance of the detector, $R_D$ = dc ohmic leakage of the dielectric, $R_L$ = input resistance of the electrometer, $E_{bb}$ = external bias for the detector and W = radiation input to the detector, (signal = $\frac{dW}{dt}$)

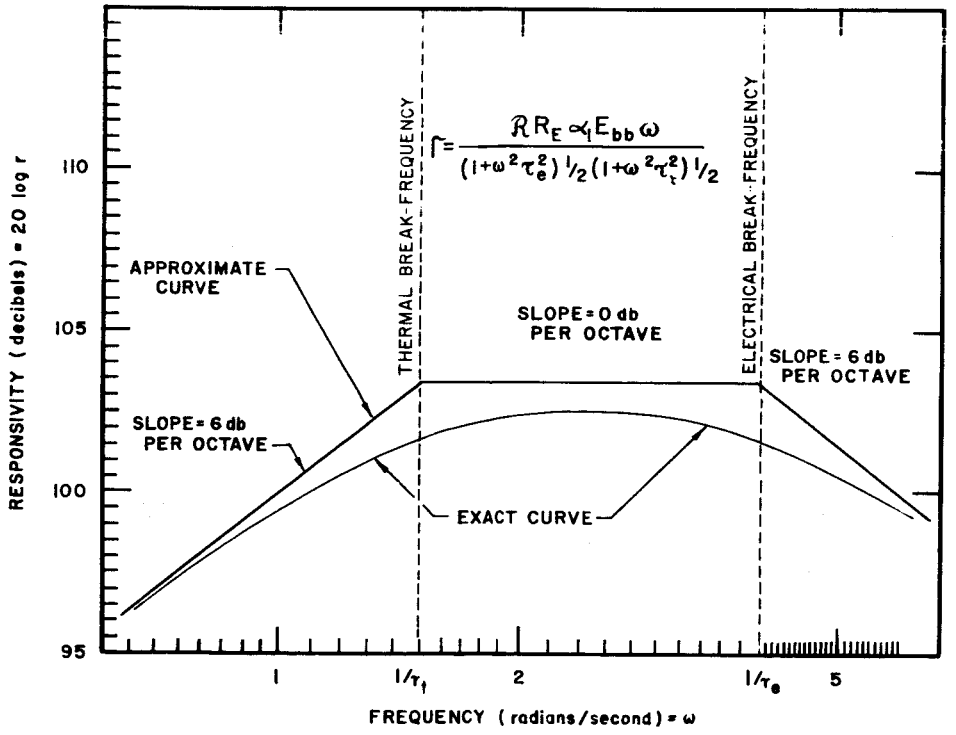


Fig. 2. Responsivity vs frequency for the ferroelectric bolometer with equivalent circuit giving in Figure 1. Typical frequency response curve drawn for a particular case $\tau_t$ = .67 sec., $\tau_e$ = .25 sec., $\Re R_E \alpha_1 E_{bb} = 10^5$.

If we take the new dependent variable

$$\theta = T - T_o - T_{dc} \tag{3}$$

where $T_{dc}$ is defined by

$$\mathcal{G}\, T_{dc} = W_h = \frac{V_{OD}^2}{R_D} \tag{4}$$

and

$$V_D = V_{OD} + \Delta V_D \tag{5}$$

Eq. (1) may be rewritten as

$$\mathcal{C}\,\frac{d\theta}{dt} + \mathcal{G}\theta = \frac{2V\Delta V_D + (\Delta V_D)^2}{R_D} + w \tag{6}$$

to the second order in $\Delta V_D$.

In writing Eq. (6) $\Delta V_D$, the time varying component of $V_D$, has been treated as infinitesimal.

In practice we shall have

$$V_D \sim 100 \text{ volts}$$

$$R_D \sim 10^{12} \text{ ohms}$$

$$\Delta V_D = rw \sim 2 \times 10^3\, w \text{ volts}$$

where r = voltage responsivity of detector.

Thus

$$\frac{2V\Delta V_D + (\Delta V_D)^2}{R_D} + w \sim (1 + 4 \times 10^{-7})\, w + 4 \times 10^{-6}\, w^2$$

Hence Eq. (6) becomes

$$\mathcal{C}\,\frac{d\theta}{dt} + \mathcal{G}\theta = w \tag{7}$$

for $w < 50$ watts (5000 watts $cm^{-2}$ for a detector of area 1 $mm^2$) to less than one per cent.

Then

$$\mathscr{C} p \theta + \mathscr{G} \theta = w \tag{8}$$

where p is the differential operator. If we take $\tau_t$ as the thermal time constant

$$\tau_t = \frac{\mathscr{C}}{\mathscr{G}} \tag{9}$$

or

$$\tau_t = \mathscr{R} \mathscr{C} \tag{10}$$

and from Eq. (8)

$$\theta = \frac{w}{\mathscr{G}(1 + p \tau_t)} \tag{11}$$

Given an expression for w, we can by transform methods find $\theta$. Since in practice the infrared signal may be sinusoidally modulated we may take

$$w = W_o e^{j\omega t} \tag{12}$$

Solving Eq. (11) for the signal given in Eq. (12), we obtain

$$\theta = \frac{\mathscr{K} W_o}{(1 + \omega^2 \tau_t^2)^{\frac{1}{2}}} e^{j(\omega t - \tan^{-1} \omega \tau_t)} \tag{13a}$$

or

$$\theta = K e^{j\omega t} \tag{13b}$$

For a unit step or Heaviside function,

$$w = W_o\, U(t) \tag{14}$$

the solution of Eq. (11) is

$$\theta = \mathcal{R} W_o \left(1 - e^{-t/\mathcal{R}C}\right) \tag{15}$$

For a ramp input,

$$w = Kt \tag{16}$$

The solution of Eq. (11) is

$$\theta = \mathcal{R}K \left[t - \tau_t \left(1 - e^{-t/\tau_t}\right)\right] \tag{17}$$

We now examine the electrical response of the network and its relation to the detector temperature and hence to the input signal.

Writing the node equation for the equivalent circuit shown in Figure 1, we obtain

$$\frac{V_D - E_{bb}}{R_L} + \frac{V_D}{R_D} + I_D = 0 \tag{18}$$

To obtain a general solution of Eq. (18), we must write an expression for $I_D$ relating this current to the pyroelectric properties of the dielectric in $C_D$.

In general, the total vector polarization $\vec{P}$ is expressed by

$$\vec{P} = \vec{P}_i + \vec{P}_s \tag{19}$$

where

$$\vec{P}_i = \chi \vec{E} \ , \tag{20}$$

$\chi$ is the electric susceptibility and $P_s$ is the spontaneous polarization.

At constant stress, the following relationship will be valid:

$$\vec{P}_s = \vec{P}_s(T) \tag{21}$$

Integrating over the standard Gaussian pillbox we have

$$Q_t = \int_s \vec{D} \cdot \vec{ds} = \int_s (\vec{E} + \vec{P}_i) \cdot \vec{ds} + \int_s \vec{P}_s \cdot \vec{ds} \tag{22}$$

where $Q_t$ is the total surface charge on each electrode.

If we assume a detector with plane parallel geometry, disregarding fringing of the field at the edge and taking the dielectric as isotropic, homogeneous and linear, we can evaluate the integrals of Eq. (22) and find,

$$Q_t = \frac{\epsilon A}{d} V_D + AP_s \tag{23}$$

where d is the thickness of the dielectric, A is the area of each electrode, and $\epsilon$ is the real part of the dielectric constant expressed by

$$\epsilon = (1 + \chi) \ \epsilon_o = K'\epsilon_o \tag{24}$$

$\epsilon_o = 8.854 \times 10^{-12}$ farad $m^{-1}$, is the electrical permittivity of free space and K' is the relative permittivity of the

dielectric. If the capacitance $C_D$ of the detector is defined by $C_D = \left.\frac{\partial Q_t}{\partial V}\right|_{\epsilon, T}$ then

$$C_D = \frac{\epsilon A}{d} \tag{25}$$

Differentiating Eq. (23) we obtain the charging current

$$I_D = C_D \frac{dV_D}{dt} + V_D \frac{dC_D}{dt} + A \frac{dP_s}{dt} \tag{26}$$

Experimental results show that $C_D$ and $P_s$ can be expanded as:

$$C_D = C_o + \alpha_1 \theta + \beta_1 \theta^2 + \gamma_1 \theta^3 + \ldots\ldots \tag{27}$$

$$P_s = P_o + \alpha_2 \theta + \beta_2 \theta^2 + \gamma_2 \theta^3 + \ldots\ldots \tag{28}$$

where $C_o$, $P_o$, $\alpha_1$, $\alpha_2$, $\beta_1$, $\beta_2$, $\gamma_1$, $\gamma_2$ ..... are constant for small $\theta$. In the linear region of the dielectric or for small $\theta$ in a non-linear region

$$C_D = C_o + \alpha_1 \theta \tag{29}$$

$$P_s = P_o + \alpha_2 \theta \tag{30}$$

Then from Eq. (26)

$$I_D = (C_o + \alpha_1 \theta) \frac{dV_D}{dt} + \alpha_1 V_D \frac{d\theta}{dt} + \alpha_2 A \frac{d\theta}{dt} \tag{31}$$

For a sinusoidally modulated infrared signal, using the expression for $\theta$ of Eq. (13b), Eq. (31) becomes

$$I_D = (C_o + \mu_1 e^{j\omega t}) \frac{dV_D}{dt} + j\omega \mu_1 V_D e^{j\omega t} + j\omega \mu_2 A e^{j\omega t} \tag{32}$$

where

$$\mu_1 = \alpha_1 K \tag{33}$$

$$\mu_2 = \alpha_2 K \tag{34}$$

Using $I_D$ of Eq. (32), the node equation (18) becomes:

$$\frac{V_D - E_{bb}}{R_L} + \frac{V_D}{R_D} + (C_o + \mu_1 e^{j\omega t}) \frac{dV_D}{dt} + j\omega\mu_1 V_D e^{j\omega t} +$$

$$+ j\omega\mu_2 A e^{j\omega t} = 0 \tag{35}$$

Eq. (35) has a series solution of the form:

$$V_D = \sum_{n=0}^{\infty} V_n e^{jn\omega t} \tag{36}$$

where

$$V_n = V_{on} e^{j\phi n} \tag{37}$$

and $V_{on}$ and $\phi n$ are real. Introducing $V_D$ of Eq. (36) into Eq. (35) we obtain:

$$\frac{E_{bb}}{R_L} = G_E \sum_{n=0}^{\infty} V_n e^{jn\omega t} + (C_o + \mu_1 e^{j\omega t}) \sum_{n=1}^{\infty} V_n nj\omega e^{jn\omega t} +$$

$$+ j\omega\mu_1 e^{j\omega t} \sum_{n=0}^{\infty} V_n e^{jn\omega t} + j\omega\mu_2 A e^{j\omega t} \tag{38}$$

where

$$G_E = \frac{1}{R_D} + \frac{1}{R_L} = \frac{1}{R_E} \tag{39}$$

If we rearrange terms and adjust summation indices:

$$\frac{E_{bb}}{R_L} = \sum_{n=0}^{\infty} G_E V_n e^{jn\omega t} + \sum_{n=1}^{\infty} j\omega (n C_o V_n + \mu_1 V_{n-1}) e^{jn\omega t} +$$

$$+ \sum_{n=2}^{\infty} j\omega (n-1) \mu_1 V_{n-1} e^{jn\omega t} + j\omega \mu_2 A e^{j\omega t} \qquad (40)$$

Equating harmonics of the same order we obtain

For n = 0

$$V_o = \frac{R_E}{R_L} E_{bb} \qquad (41)$$

For n = 1

$$V_1 = \frac{-j\omega \mu_1 R_E \left[V_o + \left(\frac{\mu_2}{\mu_1}\right) A\right]}{1 + j\omega R_E C_o} \qquad (42)$$

For n = K

$$V_K = \frac{-jK\omega \mu_1 R_E V_{K-1}}{1 + jK\omega R_E C_o} \qquad (43)$$

or

$$V_n = \frac{n! \, (-j\omega \mu_1 R_E)^n \left(V_o + \frac{\mu_2}{\mu_1} A\right)}{(1 + jn\omega R_E C_o)\,(1 + j(n-1)\omega R_E C_o) \ldots (1 + j\omega R_E C_o)} \qquad (44)$$

Therefore, the solution of Eq. (35) is

$$V_D = \left(\frac{R_D}{R_D + R_L}\right) E_{bb} + \sum_{n=1}^{\infty} \frac{n! \, (-j\omega \mu_1 R_E)^n \left(V_o + \frac{\mu_2}{\mu_1} A\right) e^{jn\omega t}}{(1+jn\omega R_E C_o)(1+j(n-1)\omega R_E C_o) \ldots (1+j\omega R_E C_o)} \qquad (45)$$

Furthermore from Eqs. (33) and (34)

$$\frac{\mu_1}{\mu_2} = \frac{\alpha_1}{\alpha_2} \tag{46}$$

and from Eqs. (13a), (13b) and (33)

$$\mu_1 = \frac{\alpha_1 \mathcal{R} W_o}{1 + j\omega\tau_t} \tag{47}$$

Thus

$$V_D = \left(\frac{R_D}{R_D + R_L}\right) E_{bb} + \sum_{n=1}^{\infty} n! \left(\frac{-j\omega\alpha_1 \mathcal{R} R_E W_o}{1 + j\omega\mathcal{R}\mathcal{C}}\right)^n \cdot \frac{\left[\left(\frac{R_D}{R_D + R_L}\right) E_{bb} + \left(\frac{\alpha_2}{\alpha_1}\right) A\right] e^{jn\omega t}}{(1 + jn\omega R_E C_o)\,[1 + j(n-1)\omega R_E C_o] \ldots [1 + j\omega R_E C_o]} \tag{48}$$

Substitution of typical values for the device parameters, shows that this series converges rapidly.

Typically for $W_o < 3 \times 10^{-4}$ watts, the detector output will be

$$V_D = \left(\frac{R_D}{R_D + R_L}\right) E_{bb} - \frac{j\omega\mathcal{R} R_E W_o\, e^{j\omega t} \left[\alpha_1 \left(\frac{R_D}{R_D + R_L}\right) E_{bb} + \alpha_2 A\right]}{(1 + j\omega\mathcal{R}\mathcal{C})\,(1 + j\omega R_E C_o)} \tag{49}$$

to better than 1% accuracy. Only the n = 1 term has been kept in Eq. (49). For higher power inputs, it will be necessary either to consider higher order harmonics, to reduce the intensity of the incident radiation by use of appropriate infrared filters, or, if only high power levels are to be measured, to design the detector to have a non-optimum voltage responsivity.

If the series in Eq. (48) is not to diverge it is required that

$$\frac{\omega \alpha_1 \mathcal{R} R_E W_o}{(1 + \omega^2 \mathcal{R}^2 \mathcal{C}^2)^{\frac{1}{2}} (1 + \omega^2 R_E^2 C_o^2)^{\frac{1}{2}}} < 1 \qquad (50)$$

which for a typical detector reduces to $W_o < 3 \times 10^{-2}$ watts. Eq. (50) would seem to give the extreme upper power input at which a given detector might be operated without filtering. However, in practice, before the higher harmonics were large enough to cause breakdown of the dielectric, the high fields would place the detector in a non-linear region of operation and $\alpha_1$ would therefore be considerably reduced.

From Eq. (49) we obtain the output voltage of the ferroelectric bolometer

$$v_D = \Delta V_D = \frac{-j\omega \mathcal{R} R_E W_o e^{j\omega t}}{(1 + j\omega \mathcal{R} \mathcal{C}) (1 + j\omega R_E C_o)} [\alpha_1 (R_D / R_D + R_L) E_{bb} + \alpha_2 A] \qquad (51)$$

For temperatures above the Curie point ($T > Tc$), we may consider $P_s = 0$ and therefore $\alpha_2 = 0$. In this case Eq. (50) becomes:

$$v_D = \frac{-j\omega \mathcal{R} R_E^2 W_o \alpha_1 E_{bb} e^{j\omega t}}{R_L (1 + j\omega \mathcal{R} \mathcal{C}) (1 + j\omega R_E C_o)} \qquad (52)$$

Thus in this case the responsivity of the ferroelectric bolometer will be:

$$r_v = \frac{|v_D|}{W_o} = \frac{\omega\ (R_E/R_L)\mathcal{R}\ R_E \alpha_1\ E_{bb}}{(1 + \omega^2\mathcal{R}^2\mathcal{C}^2)^{\frac{1}{2}}\ (1 + \omega^2 R_E^2 C_o^2)^{\frac{1}{2}}} \qquad (53)$$

In practice $R_L \ll R_D$, therefore $R_E/R_L \simeq 1$. Eq. (52) then becomes:

$$r_v = \frac{\omega\mathcal{R}\ R_E \alpha_1\ E_{bb}}{(1 + \omega^2\mathcal{R}^2\mathcal{C}^2)^{\frac{1}{2}}\ (1 + \omega^2 R_E^2 C_o^2)^{\frac{1}{2}}} \qquad (54)$$

From the expression for $V_n$ defined by Eqs. (36) and (44), we see that the ratio $\left|\frac{V_{n+1}}{V_n}\right|$ will be independent of the thermal time constant. Indeed, if we measure $|V_2|$ and $|V_1|$ we can find the electrical time constant:

$$\tau_e = \frac{1}{\omega}\ \left(\frac{\lambda^2 - 1}{1 - 4\lambda^2}\right)^{\frac{1}{2}} = R_E C_o \qquad (55)$$

where

$$\lambda = \left|\tfrac{1}{2}\left(\frac{V_2}{V_1}\right)\ \left(\frac{E_{bb}}{V_1}\right)\right| \qquad (56)$$

From Eqs. (55) and (56), a convenient estimate of the attenuation of the second harmonic is obtained.

Since $\tau_e$ must be real, it is required that $1 > \lambda > \frac{1}{2}$ and thus

$$\left|\frac{2V_1}{E}\right| > \left|\frac{V_2}{V_1}\right| > \left|\frac{V_1}{E}\right| \qquad (57)$$

Since we know $\tau_e$ it is now possible to determine $\tau_t = \mathcal{R}\mathcal{C}$ from a plot of r vs. $\omega$. If we refer to the logarithmic plot of Figure 2, we see that $\tau_e = \frac{1}{\omega \tau_e}$ and $\tau_t = \frac{1}{\omega \tau_t}$ where $\omega_{\tau_e}$ and $\omega_{\tau_t}$ are the break-frequencies of this response curve. It is noted that response will be relatively independent of frequency in the band between the thermal and electrical break-frequencies.

The response of the ferroelectric bolometer to both a unit step and a ramp is also of interest. The node equation (18) may be solved directly for these inputs. However, direct solution tends to obscure in mathematical manipulation both the physics of the device and the close relationship between the response in the frequency and time domains. Thus, rather than proceeding immediately with a direct solution of Eq. (18), we first obtain the step and ramp responses by using a generalization of Eq. (51) as the first order approximation to the network transfer function defined as

$$\mathcal{T} = \frac{v_D}{w} \tag{58}$$

The generalization of Eq. (51) is then

$$\mathcal{T} = \frac{-p\mathcal{R} R_E \left[\alpha_1 (R_D/R_D + R_L) E_{bb} + \alpha_2 A\right]}{(1 + p \tau_t)(1 + p \tau_e)} \tag{59}$$

or

$$\mathcal{T} = \frac{-\lambda p}{(1 + p \tau_t)(1 + p \tau_e)} \tag{60}$$

where p is the differential operator and

$$\lambda = \mathcal{R} R_E \left[\alpha_1 (R_D/R_D + R_L) E_{bb} + \alpha_2 A\right] \tag{61}$$

Solving for the Heaviside input of Eq. (14) we find, using the Laplace transformation,

$$V_D = \frac{\lambda W_o}{\tau_t - \tau_e} \left(e^{-t/\tau_e} - e^{-t/\tau_t}\right) + E \tag{62}$$

Thus both $\tau_e$ and $\tau_t$ may be determined by measurements of the detector's step response. Since in actual detectors $\tau_e << \tau_t$, the rise time of the output pulse will be determined by $\tau_e$ and the fall time by $\tau_t$. It is noted that when the thermal and electrical time constants are equal, the detector output will be identically zero to the first order.

$v_D$ will be a maximum at time

$$t_m = \frac{1}{\left(\frac{1}{\tau_e} - \frac{1}{\tau_t}\right)} \ln\left(\frac{\tau_t}{\tau_e}\right) \tag{63}$$

which reduces to

$$t_m = \tau_e \ln\left(\frac{\tau_t}{\tau_e}\right) \tag{64}$$

for

$$\tau_e << \tau_t.$$

A short digression on the physical meaning of Eq. (62) will be illuminating. This equation says that if $\tau_e << \tau_t$,

the output for a step input will have rise time $\tau_e$ and fall time $\tau_t$. Similarly if $\tau_t \ll \tau_e$, the output will have rise time $\tau_t$ and fall time $\tau_e$.

Physically speaking, we can regard the detector as producing free charges at the capacitor plates at a rate proportional to $\partial Td/\partial t$. This time derivative of temperature starts off at an initial maximum and decays to zero with a fall time $\tau_t$. The charges meanwhile flow through the load resistor ($R_L \ll R_D$) which is part of an RC circuit with characteristic time constant $\tau_e$ and are neutralized. It is the voltage across the load resistor produced by this current that is the output given in Eq. (62).

First consider the case $\tau_e \ll \tau_t$. Here the circuit is able to neutralize the charges faster than the detector can generate them. Thus the output builds up to its maximum value at a rate determined by the rise time $\tau_e$ and then follows the rate of production of charges very closely, decaying with a fall time $\tau_t$.

For $\tau_t \gg \tau_e$, the electric circuit cannot neutralize the charges as fast as they are produced. Thus a voltage builds up across the capacitor plates with a characteristic rise time $\tau_t$ and decays with the characteristic time constant of the circuit $\tau_e$.

For the ramp input

$$w = Kt \tag{65}$$

We find by this transform method using Eq. (60) that the

detector output will be

$$v_D = - \frac{\lambda K}{\tau_t - \tau_e} \left[ \tau_e (e^{-t/\tau_e} - 1) - \tau_t (e^{-t/\tau_t} - 1) \right] \qquad (66)$$

There are three special cases of interest. For

$$t << \tau_e, \quad t << \tau_t$$

$$v_D \simeq 0 \qquad \text{to the 1st order in time.} \qquad (67)$$

$$v_D \simeq \frac{\lambda K}{2} \left( \frac{t}{\tau_t - \tau_e} \right)^2 \qquad \text{to the 2nd order in time.} \qquad (68)$$

For

$$t >> \tau_e, \quad t << \tau_t$$

$$v_D \simeq - \lambda K \left( \frac{t - \tau_e}{\tau_t - \tau_e} \right) \simeq - \lambda K \left( \frac{t}{\tau_t} \right) \qquad (69)$$

For

$$t >> \tau_t, \quad t >> \tau_e$$

$$v_D \simeq - \lambda K \simeq - \frac{\lambda}{\mathcal{K}} \frac{\partial \theta}{\partial t} \qquad (70)$$

where we have used Eq. (17). In this last case we note that the detector output is directly proportion to the change in detector temperature per unit time.

Generalization of Eq. (51) to determine response to arbitrary inputs is easily justified on physical grounds but is not mathematically valid without further explanation. Instead of providing such mathematical justification which would not be particularly enlightening, we instead proceed to

solve Eq. (18) directly for some special cases of particular interest using a step input.

We will find that the general solution for a step input given by Eq. (62) will reduce identically to the direct solutions in each special case. From the exact correspondence between Eq. (62) and these direct solutions, we then deduce that Eq. (62) does indeed display the true response of the ferroelectric bolometer to a Heaviside input and is exact to the first order. We also conclude that our solution, given by Eq. (66), for a ramp input is similarly valid to the 1st order.

Substituting $\theta(t)$, as displayed in Eq. (15) for a unit step input, into the expression Eq. (31) for the charging current we have

$$I_D = [C_o+\alpha_1\mathcal{R}W_o(1-e^{-t/\mathcal{R}\mathcal{C}})]\frac{dV_D}{dt} - \frac{\alpha_1 W_o}{\mathcal{C}}e^{-t/\mathcal{R}\mathcal{C}}V_D + + \frac{\alpha_2 A W_o e^{-t/\mathcal{R}\mathcal{C}}}{\mathcal{C}} \tag{71}$$

Inserting Eq. (71) into the node equation (18), we obtain the exact differential equation describing the electrical response of the detector to a Heaviside input. Thus

$$\frac{E_{bb}}{R_L} - \frac{\alpha_2 A W_o}{\mathcal{C}} + \frac{\alpha_2 A W_o t}{\mathcal{R}\mathcal{C}^2} = V_D\left\{\frac{1}{R_E} - \frac{\alpha_1 W_o}{\mathcal{C}} + \frac{\alpha_1 W_o t}{\mathcal{R}\mathcal{C}^2}\right\} + + \left\{C_o + \frac{\alpha_1 W_o t}{\mathcal{C}}\right\}\frac{dV_D}{dt} \tag{72}$$

Physical reasoning and/or Eq. (62) indicate that the special cases of interest will be for $t \ll \mathcal{R}\mathcal{C}$. For such times, Eq. (72) becomes to the first order in $(t/\mathcal{R}\mathcal{C})$.

$$\frac{E_{bb}}{R_L} - \frac{\alpha_2 A W_o}{\mathcal{C}} + \frac{\alpha_2 A W_o}{\mathcal{R}\mathcal{C}^2} t = V_D \left[\frac{1}{R_E} - \frac{\alpha_1 W_o}{\mathcal{C}} + \frac{\alpha_1 W_o t}{\mathcal{R}\mathcal{C}^2}\right] + \left[C_o + \frac{\alpha_1 W_o t}{\mathcal{C}}\right] \frac{dV_D}{dt} \tag{73}$$

Equation (73) is now solved for the two special cases:

I) $T < T_c$ $\qquad \frac{\alpha_1 E_{bb}}{\alpha_2 A} \ll 1$

II) $T > T_c$ $\qquad \alpha_2 \equiv 0$

For case I, Eq. (73) reduces to

$$\frac{E_{bb}}{R_L} - \frac{\alpha_2 A W_o}{\mathcal{C}} + \frac{\alpha_2 A W_o}{\mathcal{R}\mathcal{C}^2} t = \frac{V}{R_E} + C_o \frac{dV}{dt} \tag{74}$$

which has the homogeneous solution

$$V_{DH} = K_o e^{-t/R_E C_o} \tag{75}$$

where $K_o$ is an arbitrary constant to be determined by the boundary conditions, and the particular solution

$$V_{DP} = K_1 + K_2 t \tag{76}$$

where

$$K_1 = R_E \left[\frac{E}{R_L} - \frac{\alpha_2 A W_o}{\mathcal{C}} \left(1 + \frac{C_o}{\mathcal{R}\mathcal{C}}\right)\right] \tag{77}$$

and

$$K_2 = \frac{\alpha_2 A W_o R_E}{\mathcal{R}\mathcal{C}^2} \tag{78}$$

If we apply the boundary condition,

$$V_D = E_{bb} \quad \text{at} \quad t = 0 \tag{79}$$

the full solution to Eq. (74) becomes

$$V_D = V_{DH} + V_{DP} = \left[E\left(1 - \frac{R_E}{R_L}\right) + \frac{\alpha_2 A W_o R_E}{\mathscr{C}}\left(1 + \frac{C_o}{\mathscr{R}\mathscr{C}}\right)\right] e^{-t/R_E C_o} + \tag{80}$$

$$+ R_E\left[\frac{E}{R_L} - \frac{\alpha_2 A W_o}{\mathscr{C}}\left(1 + \frac{C_o}{\mathscr{R}\mathscr{C}}\right)\right] + \frac{\alpha_2 A W_o R_E}{\mathscr{R}\mathscr{C}^2}\, t$$

Since for a typical detector $\frac{R_E}{R_L} \simeq 1$ and $\frac{C_o}{\mathscr{R}\mathscr{C}} \simeq 3 \times 10^{-11} \ll 1$ Eq. (80) reduces to

$$V_D = E + \frac{\alpha_2 A R_E}{\mathscr{C}} W_o \left\{e^{-t/\tau_e} - \left(1 - \frac{t}{\tau_t}\right)\right\} \tag{81}$$

which to the first order in $\frac{t}{\tau_t}$ is identical to the response given in Eq. (62) when the requirements $\alpha_1 = 0$ and $\tau_e \ll \tau_t$ are incorporated in that general expression.

For case II, Eq. (73) reduces to

$$\frac{E_{bb}}{R_L} = V_D\left\{\frac{1}{R_E} - \frac{\alpha_1 W_o}{\mathscr{C}} + \frac{\alpha_1 W_o}{\mathscr{R}\mathscr{C}^2}\, t\right\} + \frac{dV_D}{dt}\left\{C_o + \frac{\alpha_1 W_o t}{\mathscr{C}}\right\} \tag{82}$$

which has a series solution of the form

$$V_D = \sum_{n=0}^{\infty} V_n t^n \tag{83}$$

where the $V_n$ are constants. The expressions for the

coefficients $V_n$ are in general extremely complicated. However, for $R_L \simeq R_E$, $\tau_e << \tau_t$, $W_o < 5 \times 10^{-4}$ watts, and $t < 1$ second, the series in Eq. (83) will converge to

$$V_D = E + \frac{\alpha_1 W_o E_{bb}}{\mathscr{C}} (1 - e^{-t/\tau_e}) \qquad (84)$$

for $t << \tau_t = \mathscr{R}\mathscr{C}$. When the assumptions made in deriving Eq. (80) are applied to Eq. (62), we see that the two expressions for step response in the region $T > T_c$ are identical. We therefore deduce that Eq. (62) is the valid expression for the first order response of the ferroelectric bolometer to a step input of magnitude $W_o < 3 \times 10^{-4}$ watts. We note that Eq. (62) is valid both above and below the Curie point. We make a similar conclusion about Eq. (66), the response to a ramp input.

For our Heaviside input, maximum output of the detector will occur when $\tau_e << \tau_t$; then

$$\mathscr{V}_{max} = \frac{\lambda W_o}{\tau_t} = \frac{(\alpha_1 E_{bb} + \alpha_2 A) R_E}{\mathscr{C}} W_o \qquad (85)$$

For power inputs above $5 \times 10^{-4}$ watts we expect non-linear effects in the detector to become significant, probably in the form of higher order transients, i.e.,

$$e^{-2t/\tau_e}, \quad e^{-3t/\tau_e} \ldots\ldots$$

Hence for high signal levels we may expect significantly shorter rise times than $\tau_e$.

The voltage responsivity of the detector will be

$$r_{v,step} = \frac{(\alpha_1 E_{bb} + \alpha_2 A)}{\mathscr{C}} R_E \text{ volt watt}^{-1} \qquad (86)$$

and the current responsivity

$$r_{I,step} = \frac{(\alpha_1 E_{bb} + \alpha_2 A)}{\mathscr{C}} \text{ ampere watt}^{-1} \qquad (87)$$

It is important to note that the current responsivity depends only on the applied bias and the characteristics of the device itself and not on the electrical parameters of the associated electronics. This is of course provided $\tau_e << \tau_t$.

Equations (51) and (85) would seem to indicate that for $T > T_c$ the detector responsivity r is directly proportional to the bias voltage ($E_{bb}$). This will be true, however, only for the linear region of the detector where $\alpha_1 \simeq$ constant (and where $\omega < \frac{1}{\tau_e}$ for a sinusoidal input).

In general, the dielectric constant and hence both C and $\alpha_1$ will be functions of the stresses introduced by the electric field originated by $E_{bb}$. An increase in electric field will decrease the dielectric constant. A plot of the relation between the relative permittivity (K') and the electric field E for a material similar to the type used in our detectors is found in Figure 3.

The optimum value of $E_{bb}$ to be used is decided on the basis of maximizing the responsivity. Other analyses have indicated dielectric breakdown to be the limiting factor; however, it is indeed the field dependence of $\alpha_1$ and C that will determine the point of operation. The electric fields

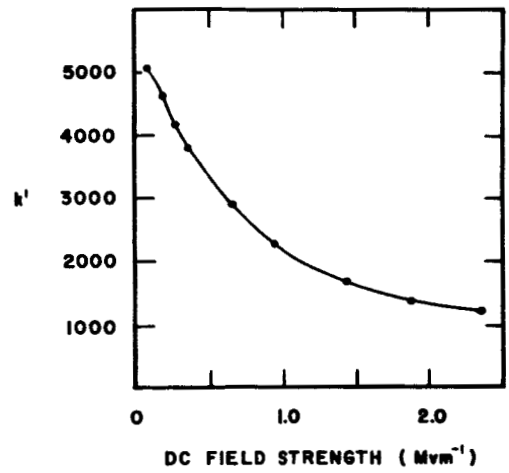


Fig. 3. Field strength dependence of permittivity for barium-strontium titanate ceramic (25% $SrTiO_3$, 75% $BaTiO_3$) at 25°C measured at 400 Kcps with dc bias. ("Dielectric and Piezoelectric Properties of Barium Titanate", Phy. Rev. 71, 892, 1947).

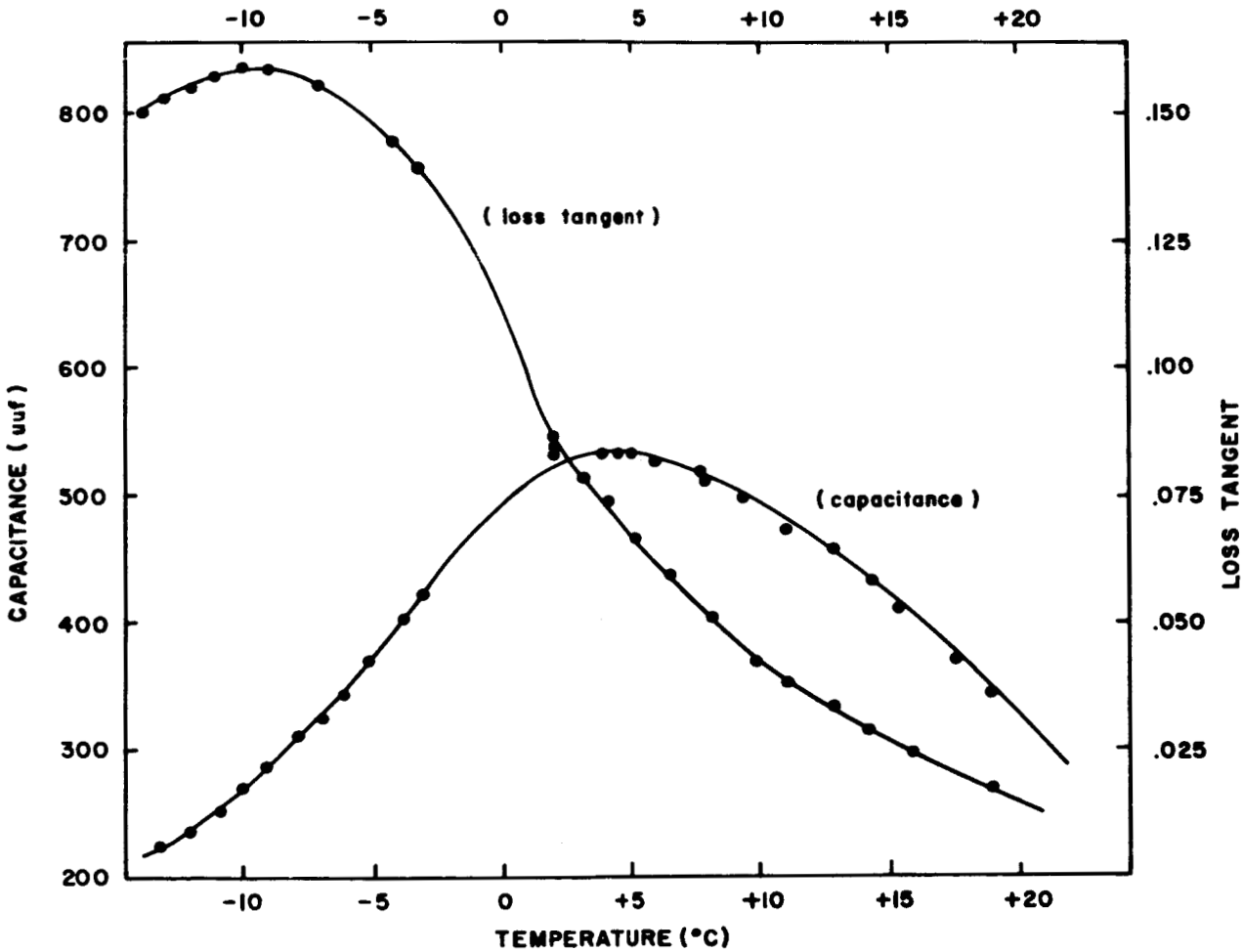


Fig. 4. Capacitance $C_D$ and loss tangents as a function of temperature for the ferroelectric bolometer, serial #G-20311. Measurements at a frequency of 1 Kcps and a field strength of 100 volt $cm^{-1}$.

used in our detectors range from $.5 \times 10^6$ volts/meter to $1.6 \times 10^6$ volts/meter. Referring to Figure 3, we see that at these field strengths, K' has decreased to 65% and 30% of its zero field value respectively.

The thermal point of operation of the detector depends on the characteristics of the ferroelectric material itself. In the case of material with the characteristics given in Figure 4, above the Curie point the detector will operate at practically constant responsivity from $10^o$ to $25^oC$ (provided $\omega << \frac{1}{\tau_e}$ throughout this range if the input is sinusoidal).

To evaluate the responsivity of the detector we introduce parameters corresponding to the operational ferroelectric bolometer listed in Table II under Serial # G-20311. The detector is cooled by radiation through a black layer (emissivity = 1) on its upper surface and by conduction through the glass backing and leads. The effect of cooling by radiation can be expressed mathematically by a radiation conductance ($\mathscr{G}_r$) that a room temperature will have the value

$$\mathscr{G}_r = 5.8 \times 10^{-6} \text{ watts } {}^oC^{-1}$$

The lead conductance will be inversely proportional to the square root of the chopping frequency and at 10 cps:

$$\mathscr{G}_\ell = 5.6 \times 10^{-7} \text{ watts } {}^oC^{-1}$$

Furthermore for the bolometer #G-20311 the thermal conductance due to heat transfer through the flake base to the glass backing will be approximately

$$\mathcal{G}_b = 1 \times 10^{-3} \text{ watt } {}^{o}C^{-1}$$

if we assume a linear gradient across the detector flake and the cement bonding the flake and the glass. Thus the predominant cooling in this detector is due to $\mathcal{G}_b$ and the total thermal resistance is

$$\mathcal{R} = 1 \times 10^{3} \text{ watt}^{-1} \ {}^{o}C$$

For the heat capacity $\mathcal{C}$ of the detector #G-20311 we consider only the contribution of the dielectric mass and neglect mass of the electrodes, black layer, and the equivalent heat capacity due to the glass backing.

Taking the specific heat of the dielectric to be $C_p$ = 0.12 cal $g^{-1}$ ${}^{o}C^{-1}$,* we find $\mathcal{C} = 5 \times 10^{-4}$ joules ${}^{o}C^{-1}$.

With these values we obtain a thermal time constant

$$\tau_t = \mathcal{R}\mathcal{C} = 0.5 \text{ second}$$

Experimentally, we found $\tau_t$ = 4 seconds. Because of the many assumptions and estimates of physical quantities involved in the computation of $\mathcal{C}$ and $\mathcal{R}$ we consider these two values to be in reasonable agreement.

By direct measurement we also obtained the electrical time constant for the point of operation indicated in Table II:

$$\tau_{e,\text{experimental}} = 70 \text{ milliseconds}$$

---

*A. G. Chynoweth, "Dynamic method for measuring the pyroelectric effect with special reference to Barium Titanate," J. Appl. Phys., 27, 78, 1956.

The equivalent load resistance $R_L$ is determined by the real part of the equivalent input impedance of the electrometer. The electrometer employed is a Keithley #417 with a rise time of about 230 milliseconds for 300 $\mu\mu$f* input capacitance. This value is for operation on the $10^{-12}$ mp range, full scale. For the range $10^{-11}$ amp and the same input capacitance the rise time will be reduced by a factor of ten. Moreover, on the same range scale for different settings of the multiplier, different rise times will be obtained.

Taking the capacitance $C_D$ of the detector, 140 $\mu\mu$f measured at 28.5°C, and the measured rise time of 70 milliseconds, we estimate:

$$R_L \simeq \frac{70 \times 10^{-3} \text{ seconds}}{21 \times 10^{-11} \text{ farads}} = 3.3 \times 10^8 \text{ ohms}$$

Since

$$R_D \simeq 10^{12} \text{ ohms}$$

$$R_E \simeq R_L = 3.3 \times 10^8 \text{ ohms}$$

Extrapolating measurements from the measurements of $C_D$ vs. T (Fig. 4), we obtain for the detector #G-20311 at 28.5°C

$$\alpha_1 = 1.6 \times 10^{-11} \text{ farads } {}^{o}C^{-1}$$

Noting that $\tau_t = 0.5$ second is much greater than $\tau_e = 70$ milliseconds, and that Eq. (86) is valid, we

*Keithley Instruments, "Instruction Manual Model #417 Picoammeter," 1963.

obtain the voltage responsivity to an infrared step function

$$r_{v,\text{theoretical}} = 3.5 \times 10^{3} \text{ volt watts}^{-1}$$

The voltage responsivity obtained experimentally under the same conditions is

$$r_{v,\text{experimental}} = 2.33 \times 10^{3} \text{ volt watts}^{-1}$$

This is 66% of the theoretical responsivity just computed. Since the particular detector on which those measurements were made had a black layer of camphor soot that did not completely cover the detector surface, it is not unreasonable to conclude that the device was working at less than 70% of theoretical efficiency. Noting the approximations which have been made in this analysis and possible instrumental sources of error such as that due to the spectral convolution between the detector window transmittance and black body emittance of the radiation source, we find this agreement between the experimental and theoretical responsivities to be extremely good.

If we take into account this reduction in efficiency, we have

$$r_{I,\text{theoretical red.}} \cong r_{I,\text{experimental}} = 7 \times 10^{-6} \text{ ampere watts}^{-1}$$

where

$$r_{I,\text{theoretical}} = 10.6 \times 10^{-6} \text{ ampere watts}^{-1}$$

## EXPERIMENTAL RESULTS

We will describe some of the experimental results for one ferroelectric bolometer operating in the dielectric mode. This bolometer is made of $Ba(Ti,Sn)O_3$ solid solution with a Curie point at approximately $+5^{o}C$. The bolometer is identified with the Serial #G-20311 and the relevant physical data are given in Table II.

The bolometer was tested at an infrared bench where a square wave signal at a continuously variable frequency or a step function could be generated.

Figure 5 gives the block diagram of the electronic system for testing the ferroelectric bolometer in dc and ac operation. The rise time of the electrometer for the actual working conditions is 70 milliseconds. The General Radio Vibration Analyzer provides a very narrow bandpass that is a percentage of the tuning frequency.

Figure 6 shows an actual ferroelectric bolometer flake 0.50 mm x 0.50 mm size and 50 microns thickness, Figure 7-a shows a complete bolometer, and 7-b an exploded view of the same bolometer. Figure 8 shows the response of the detector #G-20311 to a negative and positive infrared step function. The bias is 330 volts, the room temperature $28.5^{o}C$* and the step signal $7.5 \times 10^{-8}$ watts. The chart speed is 1 mm per second; noise level determined by the electronics. The record in Figure 9 was obtained under the same conditions as the one shown in Figure 8, but with a step signal of $3.3 \times 10^{-8}$ watts. The record in Figure 10 was made under the same conditions as

*The room temperature was undesirably high, due to a malfunction in the air conditioning system.

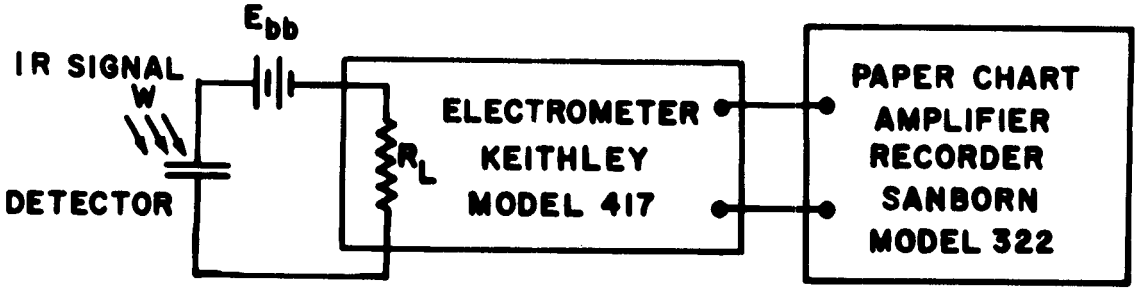


a) D.C. MODE OF OPERATION

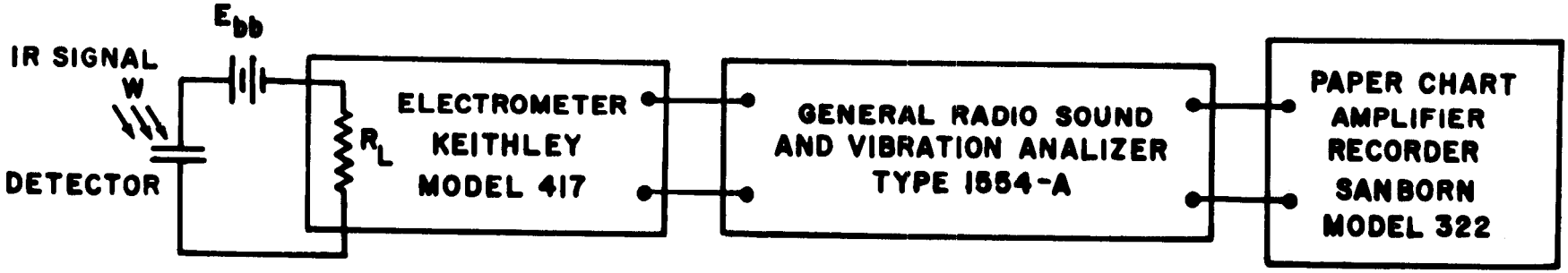


b) A.C. MODE OF OPERATION

Fig. 5. Block diagrams of the electronic setup for testing the ferroelectric bolometer; a) dc mode of operation, b) ac mode of operation.

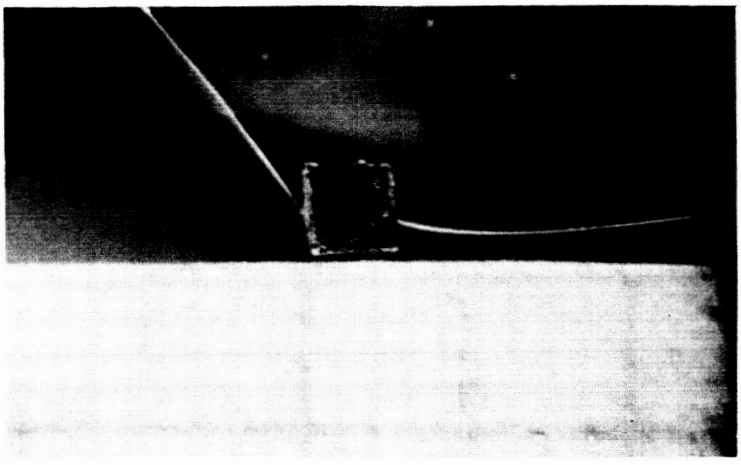

Fig. 6. Ferroelectric bolometer flake 0.50mm x 0.50mm in size and 50 microns thickness. The reticle 1.0mm x 1.0mm is for comparison purposes.

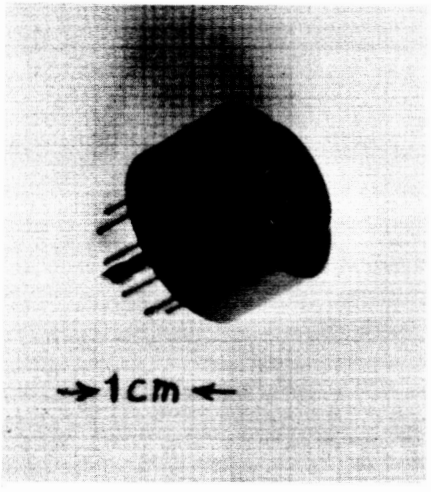


(a)

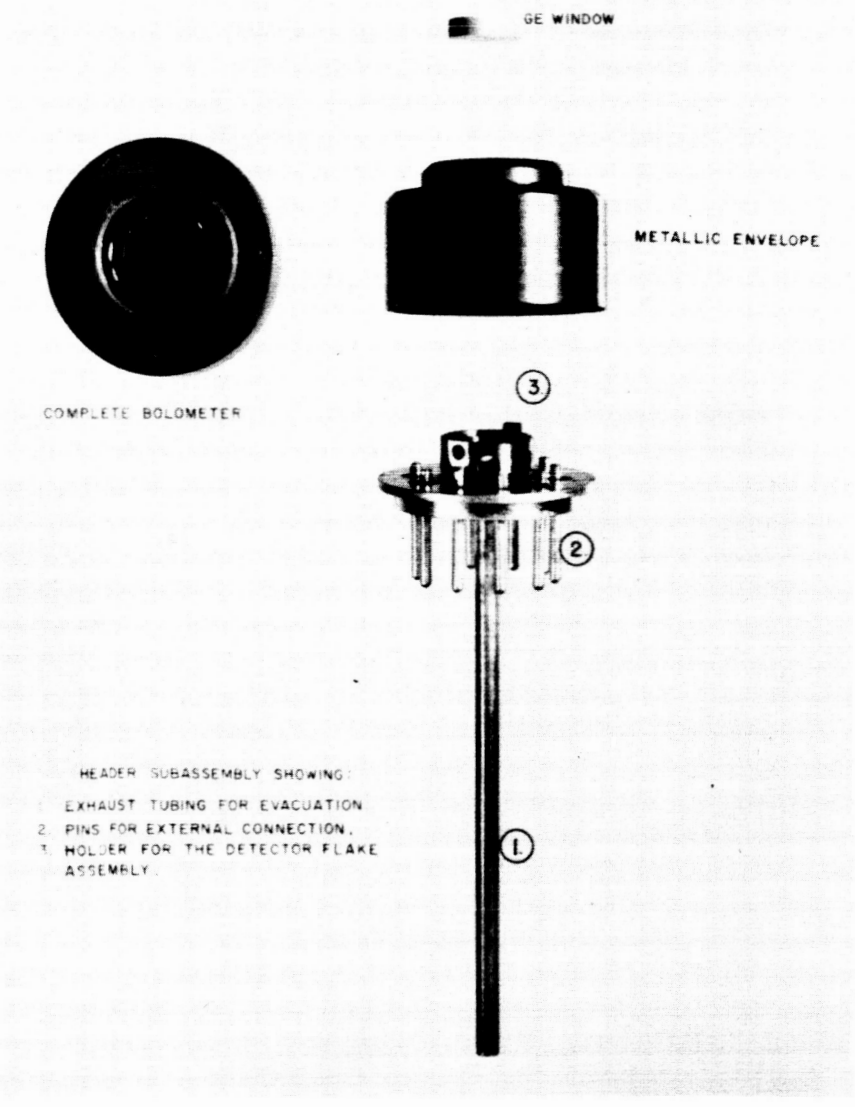


Fig. 7. a) A complete ferroelectric bolometer. b) An exploded view of the bolometer.

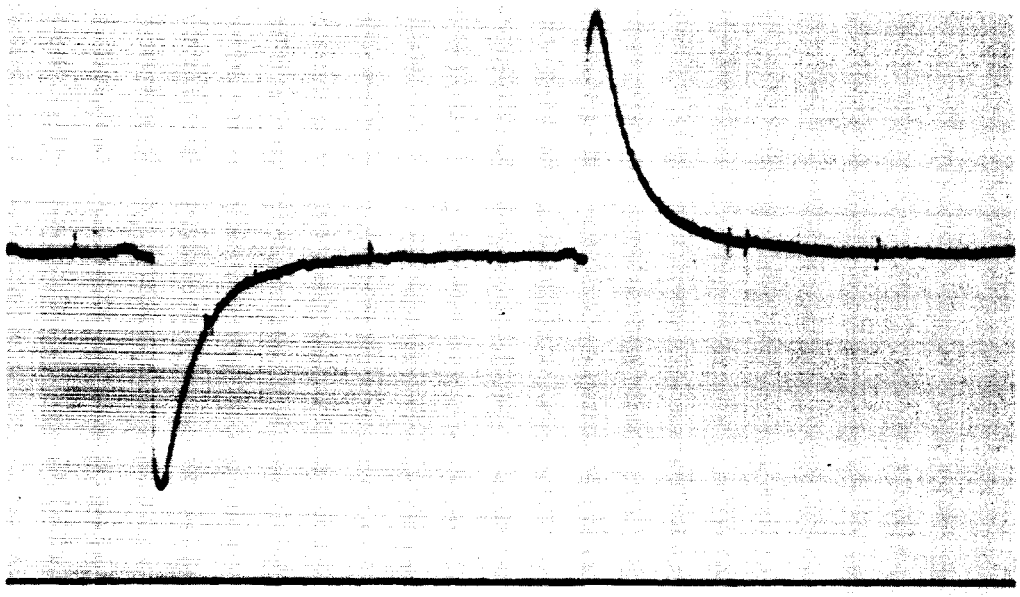

Fig. 8. Output of the detector #G-20311 in dc operation to a negative and positive infrared step function. The bias is 330 volts, the room temperature 28.5°C and the step signal $7.5 \times 10^{-8}$ watts. The chart speed is 1mm per second, noise level determined by the electronics.

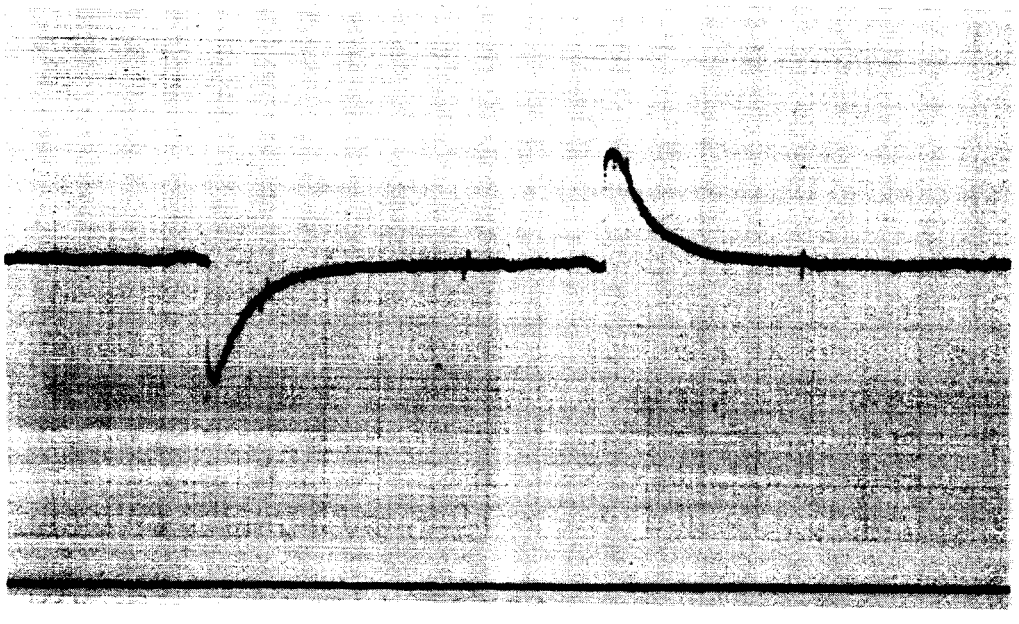

Fig. 9. This record was obtained under the same conditions as the one in Figure 8, but with a step signal of $3.3 \times 10^{-8}$ watts.

TABLE II

CHARACTERISTICS OF A FERROELECTRIC BOLOMETER
(SERIAL NO. G-20311) DEVELOPED AT HARVARD COLLEGE OBSERVATORY

| | | |
|---|---|---|
| Size (mm x mm) | | 1.0 x 1.0 |
| Thickness of Dielectric (mm) | | 0.2 |
| Material | | $Ba(Ti,Sn)O_3$ |
| Curie Temperature ($^oC$) | | +5 |
| Electrodes | | Silver |
| Black Layer | | Camphor Soot |
| Backing | | Glass |
| Lead | Material | Pt |
| | Diameter (microns) | 12 |
| | Length (mm) | 5 |
| Capacitance ($\mu\mu f$) | | 140* |
| Thermal Time Constant (sec) | Computed | 0.5 |
| | Measured | 4.0 |
| External Bias (volt) | | 330 |
| Operating Field (volt $cm^{-1}$) | | $1.65 \times 10^4$ |
| Pressure (mm Hg) | | $5 \times 10^{-5}$ |
| Window | | $BaF_2$ |
| Current responsivity amp $watt^{-1}$ | Computed | $10.6 \times 10^{-6}$ |
| | **Measured | $7 \times 10^{-6}$ |
| Voltage responsivity volt $watt^{-1}$ | Computed | $3.5 \times 10^3$ |
| | **Measured | $2.33 \times 10^3$ |
| Electrical Time Constant (sec) | Measured | 0.070 |
| Load Resistor (ohm) | +Computed | $3.3 \times 10^8$ |

*Extrapolated value for $28.5^oC$ measured at 1 Kcps and 100 volt cm-1 field strength.

**Responsivity for step input signals.

+Computed on the basis of the measured rise time.

in Figure 8, but for a step signal of $1.3 \times 10^{-8}$ watts.

Figure 11 shows the output of the bolometer #G-20011 in ac operation. The signal input is a $5.8 \times 10^{-9}$ watts peak-to-peak square wave. Chopping frequency is 2.5 cps; bandwidth, 0.25 cps; chart scale, approximately $3.2 \times 10^{-10}$ watts per division. The noise level is seen as slow fluctuations in output amplitude.

Figure 12 shows the output of the bolometer under the same conditions as in Figure 11 but with the detector "looking" at a constant temperature target; this is the noise level of the system. The equivalent noise power is $4.2 \times 10^{-10}$ watts for $\Delta f = 0.25$ cps.

In Figure 13, bandwidth is again 0.25 cps and chopping frequency, 2.5 cps. Here the chopper has been stopped suddenly and we see a decay time of 4 seconds because of the bandpass filter.

At $32^{o}C$ room temperature and with a bias of 120 volts on the same detector, we obtained a new series of oscillograms in dc and ac modes of operation. Figure 14 shows the output signal from the bolometer at a sweep speed of 2.2 and 0.5 seconds per cm for positive and negative step input signals.

In Figure 15 the operation is the same except that the sweep speed is now .2 seconds $cm^{-1}$. Figure 16-a shows the response for chopping frequencies of 0.78 cps, 1.56 cps and 3.3 cps respectively.

The response for a 6.2 cps chopping speed is shown in Figure 16-b.

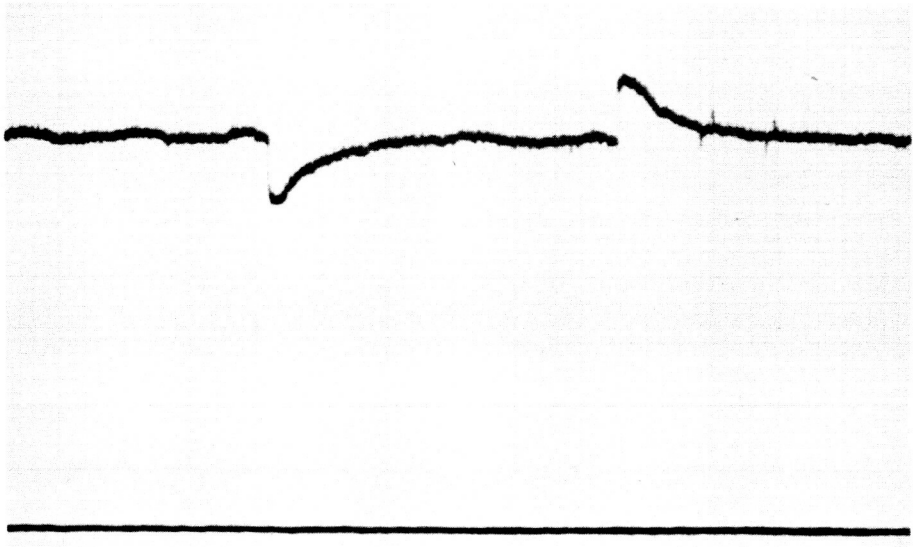

Fig. 10. This record was obtained under the same conditions as the one in Figure 8, but for a step signal of $1.3 \times 10^{-8}$ watts.

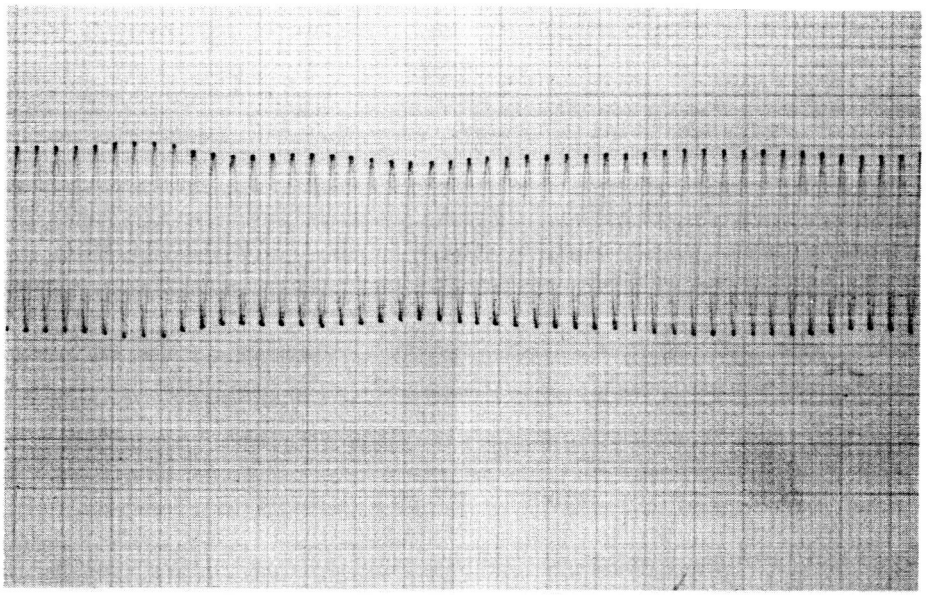

Fig. 11. Output of the detector #G-20311 in ac operation. The bias is 330 volts, the signal input is $5.8 \times 10^{-9}$ watts peak-to-peak square wave. Chopping frequency is 2.5 cps; bandpass 0.25 cps; chart scale, approximately $3.2 \times 10^{-10}$ watts per division. The noise level is seen as slow fluctuations in output amplitude.

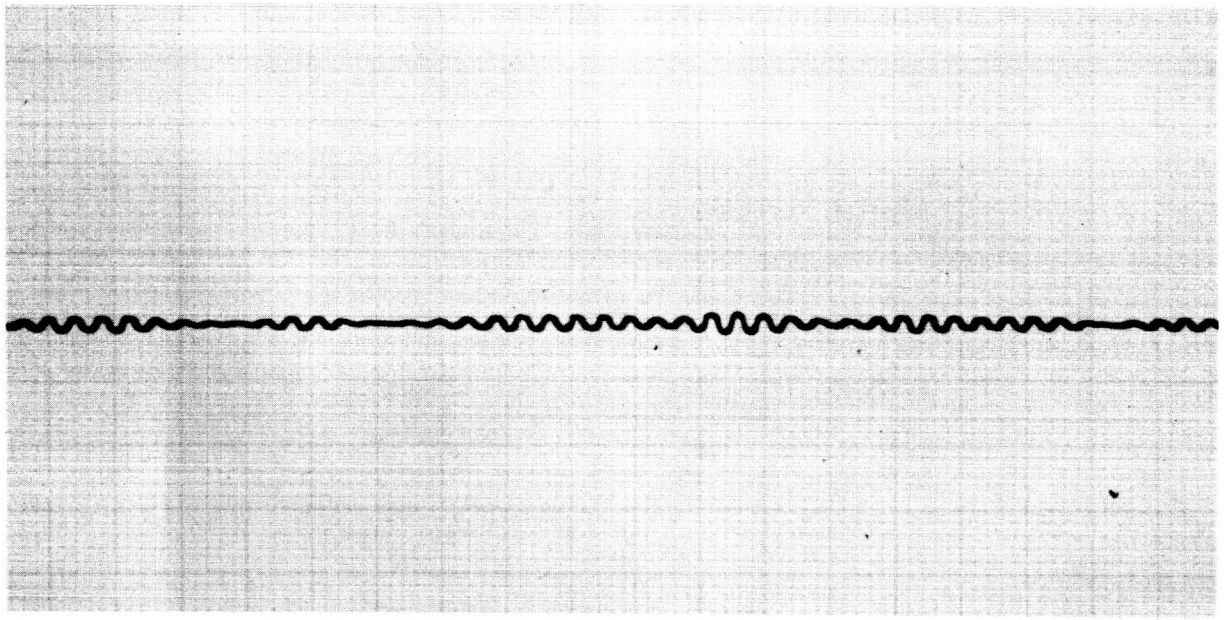

Fig. 12. Output of the detector "looking" at a constant temperature target; the same operating conditions as for Figure 11. The equivalent noise power is $4.2 \times 10^{-10}$ watts for $\Delta f = 0.25$ cps.

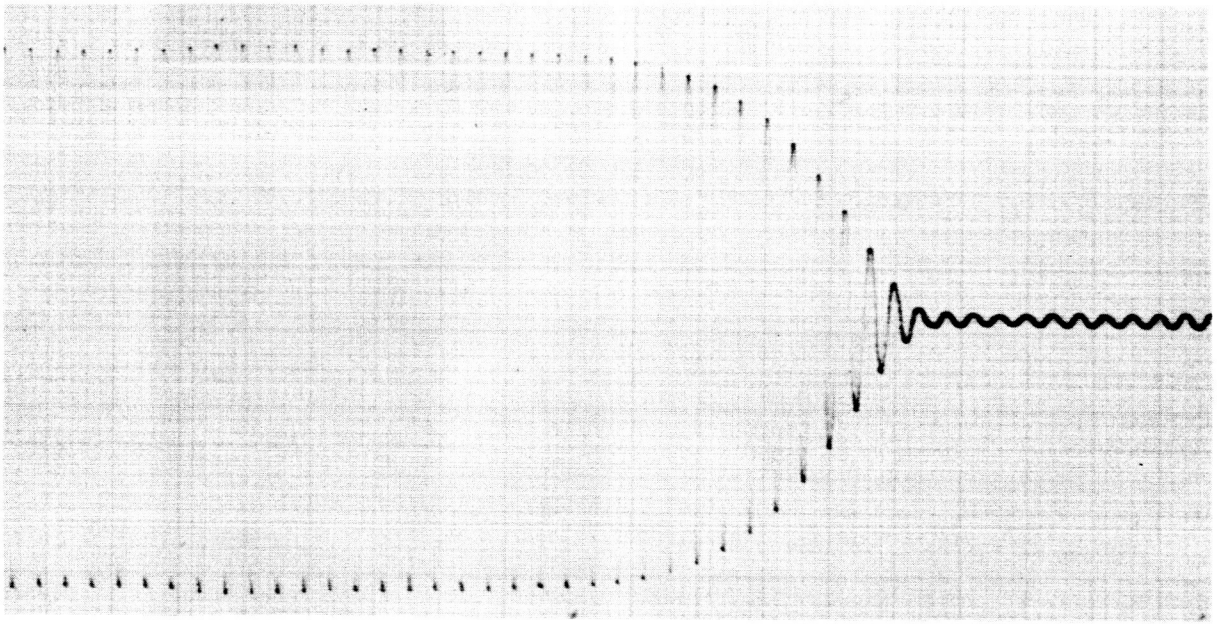

Fig. 13. Output when the chopper blade has been stoped suddenly. We see a decay time of 4 seconds because of the bandpass filter.

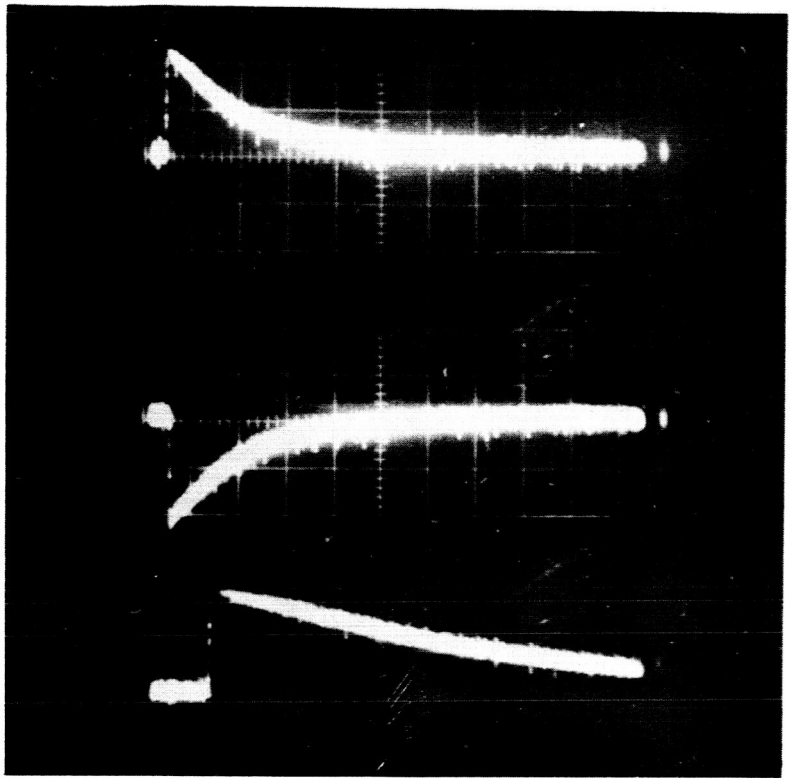

Fig. 14. Output of the detector#G-30211. The bias is 120 volts and the room temperature, 32°C. The sweep speed is 2, 2, and 0.5 seconds per cm respectively. The input signals are positive and negative steps.

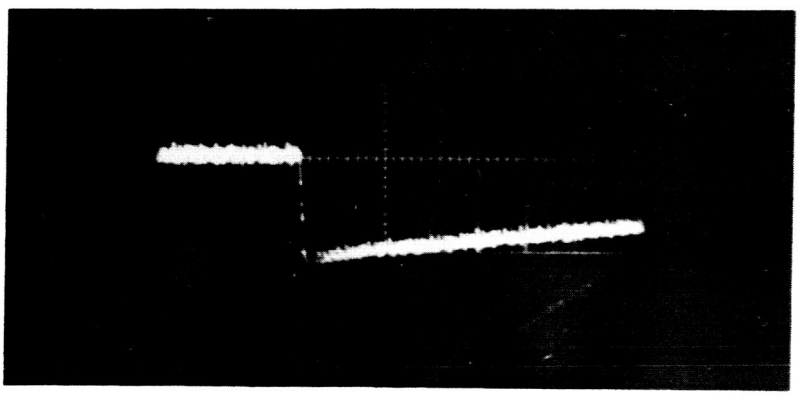

Fig. 15. The operation is the same as the one used in Figure 14, but the sweep speed is .2 seconds per cm.

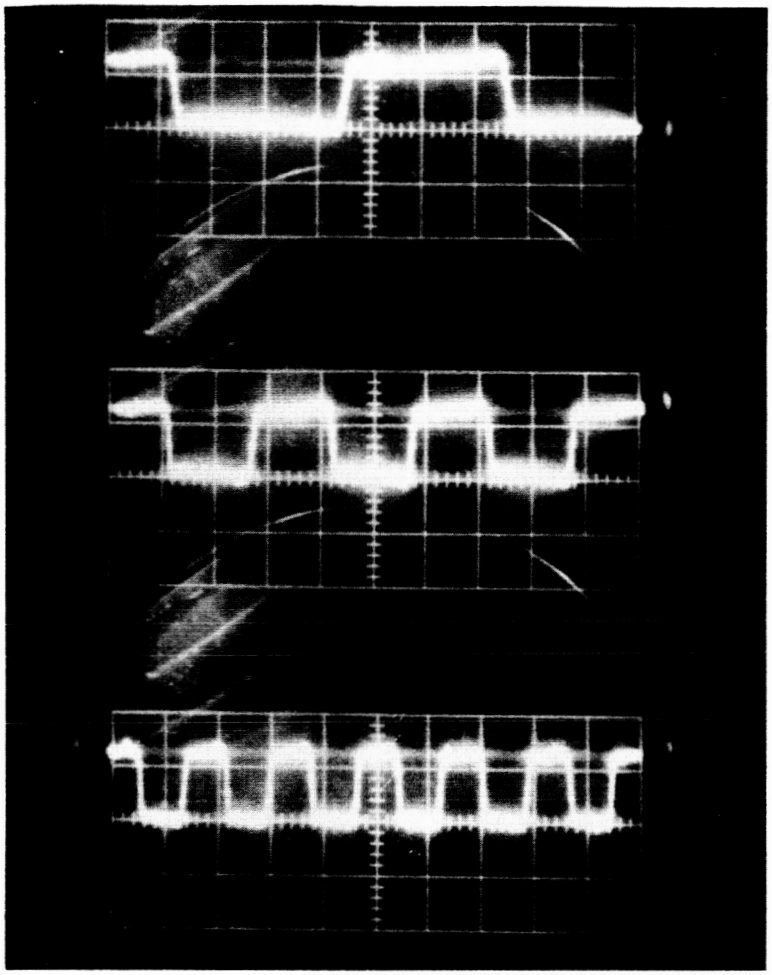

(a)

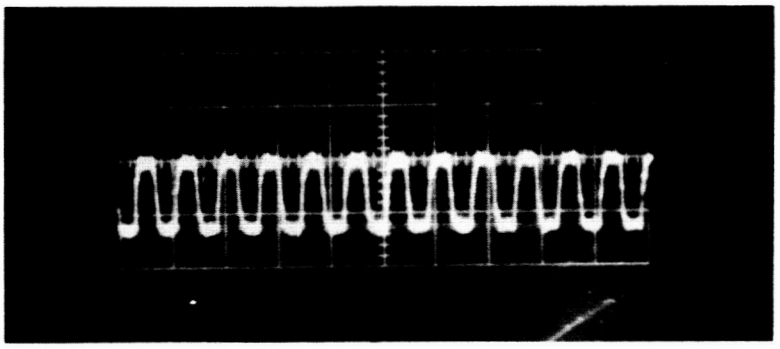

(b)

Fig. 16. a) Output for chopping frequencies of 0.78 cps, 1.56 cps, and 3.3 cps, respectively. The conditions of operation are the same as in Figure 14. b) Output for chopping frequency of 6.2 cps.

## NOISE ANALYSIS

The minimum detectable input power will be determined by the noise inherent in the ferroelectric detector element and its associated electronics. Temperature (thermal fluctuation), Johnson, shot, flicker, partition, current, and Barkhausen noise require consideration.[9, 14, 15] For a properly designed electrometer, only noise that originates in the electrometer tube itself or in the input resistor will be significant.

It is convenient to define the minimum detectable power by

$$W_m^2 = W_T^2 + r_v^{-2} \mathcal{V}_N^2 \tag{88}$$

or equivalently

$$W_m^2 = W_T^2 + r_I^{-2} i_N^2 \tag{89}$$

where

$W_T$ = rms noise power due to thermal fluctuations (temperature noise).

$r$ = detector responsivity.

$\mathcal{V}_N$ = rms noise voltage because of all electrical sources.

$i_N$ = rms noise current because of all electrical sources.

$W_m$ = rms minimum detectable power.

Although it is possible to detect signals smaller than $W_m$, the minimum detectable power as defined will serve as a good figure of merit for the system.

For a body in thermal equilibrium and exchanging heat with its environment by radiation process only

$$W_T^2 = 4KT^2 \gamma_r \Delta f \qquad (90)$$

where

K = Boltzmann's constant

$\gamma_r$ = thermal conductivity due to radiation, and

$\Delta f$ = bandwidth

Assuming that $\gamma_r$ may be generalized to include conduction processes and taking $\gamma = 10^{-3} \frac{\text{watts}}{C^o}$, $T = 302^oK$, and $\Delta f = .25$ cps, we find $W_T = 3.6 \times 10^{-11}$ watts.

Johnson noise will be given by

$$\tilde{e}_J^2 = \frac{4KT\ R_e\ \Delta f}{1 + (\omega R_e C)^2} \qquad (91)$$

which for $R_e = 3.3 \times 10^8$ ohms and $R_e C = 7 \times 10^{-2}$ seconds yields $\tilde{e}_J = 7.9 \times 10^{-7}$ volts or for $r_v = 2.33 \times 10^3$ volts watt$^{-1}$ $W_J = 3.4 \times 10^{-10}$ watts where $W_J$ is the rms power equivalent to the Johnson noise voltage $\tilde{e}_J$.

Although the Keithley #417 Electrometer uses a Raytheon CK5886 electrometer tube, the new electrometer we are constructing used an improved version, the Raytheon CK587, operated as a pentode. Our calculations will be for this latter tube. Advantages of the latter tube are lower grid current, smaller size, and lower filament dissipation.

Anode shot noise and partition noise may be considered together as the reduced shot effect.[16] The noise arising from these sources may be represented in terms of an equivalent noise resistor in the grid circuit whose value is given by

$$R_{eq} = \frac{2.5\ I_p}{G_m\ I_s}\left(1 + 8\ \frac{I_2}{G_m}\right) \qquad (92)$$

where*

$G_m$ = transconductance = $14 \times 10^{-6}$ mho

$I_p$ = plate current = $6 \times 10^{-6}$ amp

$I_2$ = screen grid current = $2.5 \times 10^{-6}$ amp

$I_s$ = space current = $8.5 \times 10^{-6}$ amp

Thus $R_{eq} \approx 3.1 \times 10^{5}$ ohms and since

$$v_{rs}^2 = 4KT\ R_{eq}\ \Delta f, \qquad (93)$$

$$v_{rs} = 3.6 \times 10^{-8} \text{ volts}$$

and

$$W_{rs} = 1.5 \times 10^{-11} \text{ watts}$$

where $W_{rs}$ is the rms power equivalent of the reduced shot noise voltage.

Grid current noise due to variations in the grid current caused by the shot effect may be calculated from

$$i_g^2 = 2e\ (I_g^+ + I_g^-)\ \Delta f \qquad (94)$$

where

$i_g$ = rms grid current noise

$e$ = electron charge ($1.6 \times 10^{-19}$ coulombs)

$I_g^-$ = electron grid current

$I_g^+$ = ionic grid current

and where $I_g^-$ and $I_g^+$ are taken as positive quantities.

---

*Measurements supplied by Raytheon Company.

TABLE III

THEORETICAL NOISE POWERS FOR A CERAMIC $Ba(Ti,Sn)O_3$ FERROELECTRIC BOLOMETER

| Source | Noise* (watts rms) |
|---|---|
| Thermal | $.36 \times 10^{-10}$ |
| Johnson | $3.4 \times 10^{-10}$ |
| Reduced Shot (anode shot and partition) | $.15 \times 10^{-10}$ |
| Grid Current (Shot) | $.02 \times 10^{-10}$ |
| Flicker | $.43 \times 10^{-10}$ |
| Battery | Below $1.0 \times 10^{-10}$ |
| Current Barkhausen | To be determined |
| Minimum Detectable Power | $4.2 \times 10^{-10}$ |

*Values for a bandpass $\Delta f = 0.25$ cps.

At the given operating potentials, total grid current $I_g = -I_g^+ + I_g^-$ will be $2 \times 10^{-15}$ amperes for pentode operation. It is estimated* that at the operating potentials $I_g^- < \frac{1}{5} I_g^+$. Taking this relation as an equality we have

$$I_g^+ + I_g^- \simeq 2.5 \times 10^{-15} \text{ amp}$$

and

$$i_g \simeq 1.4 \times 10^{-17} \text{ amp}$$

or equivalently

$$W_g = 2 \times 10^{-12} \text{ watts}$$

Since the cathode of the CK587 is oxide coated, the spectral density of flicker noise at the grid may be given by

$$\mathcal{V}_f^2 = \frac{10^{-13}}{f} \Delta f \qquad (95)$$

where $\mathcal{V}_f$ = rms flicker noise voltage. Thus

$$\mathcal{V}_f \simeq 10^{-7} \text{ volts}$$

and

$$W_f \simeq 4.3 \times 10^{-11} \text{ watts}$$

Additional noise sources would include the dielectric analog of Barkhausen noise associated with the domain walls, current noise due to fluctuations of the resistance of the dielectric, and battery noise due to fluctuations in the bias potential. Both the Barkhausen and current noises warrant further investigation. However, the Barkhausen noise will

---

*Tomasz Jedrzejewicz, Raytheon Company, Industrial Components Division, private communication.

not be important above the Curie point because of the absence of domain walls.

The battery noise is below an equivalent power of $1.0 \times 10^{-10}$ watts as determined by direct measurement of the circuit noise with and without the battery connected. Since in this measurement a dummy detector was substituted for the actual one, we cannot yet say anything about the current noise.

If we assume that these last three noise sources are minor, the theoretical minimum detectable power for the detector analyzed will be $W_m \simeq 3.5 \times 10^{-10}$ watts. The minimum detectable power for the detector under analysis is determined mainly by Johnson noise. From Eqs. (53) and (91) we have

$$W_J^2 = \frac{\mathcal{V}_J^2}{r_v^2} = \frac{4KT\ \Delta f}{R_e} \frac{\left(1 + \frac{1}{\omega^2 \tau_t^2}\right)}{(\alpha_1 E_{bb} + \alpha_2 A)^2} \qquad (96)$$

for $R_D >> R_L$ which reduces for $\tau_t >> \tau_e$ and $\omega \tau_t >> 1$ to

$$W_J^2 = \frac{4KT\ \Delta f}{r_{I,step}^2} \left(\frac{1}{R_e}\right)$$

if we use Eq. (87). Thus, at constant temperature $W_J$ may be reduced by increasing $R_e$ or by using an electrometer with slower response ($\tau_e = R_e C$ and C is determined almost entirely by the external circuit). Thus unless it is possible to improve the responsivity, $r_{I,step}$, we must compromise between minimizing Johnson noise and minimizing $\tau_e$.

## IMPROVEMENT OF RESPONSIVITY

We show that it might be possible to improve $r_{I,step}$ in future detectors.

Using Eq. (30)

$$\mathscr{C} = \rho A \, dC_p \tag{97}$$

and

$$\alpha_1 = \frac{A}{d} \frac{\partial \epsilon}{\partial T} \tag{98}$$

where

$\rho$ = mass density

$C_p$ = specific heat (heat capacity per unit volume)

we rewrite Eq. (87)

$$r_{I,step} = \frac{1}{d \rho C_p} \left( \frac{E_{bb}}{d} \frac{\partial \epsilon}{\partial T} + \frac{\partial P}{\partial T} \right) \tag{99}$$

Thus for a given material, responsivity at a constant electric field will be increased by reducing the thickness (d) of the detector flake.

Since the surface of the ceramic that we use has a granular structure, the thickness will depend mainly on our ability to produce electrodes on each side of the detector without short-circuiting the two electrodes through the ceramic flake. At this point we have found it practical to reduce the thickness of the detector flake to 50 microns. In accordance with Eq. (87), at this thickness for the same material and operating conditions, the responsivity will increase by a factor of 4 compared with that obtained with

the detector#G-20311; this means that the equivalent input noise is also reduced by the same factor.

To evaluate the astronomical possibilities of this detector, for example in planetary astronomy, let us consider signal levels. We will assume the use of a reflecting telescope with an equivalent reflectivity of 65%, an f-number of 5.5, observing through the atmospheric window $8\mu$ -$14\mu$ and 7 mm of precipitable water. Under these observing conditions for a planet at a black body temperature of $173^{o}K$ the increment of irradiance H per degree Kelvin will be $5.2 \times 10^{-10}$ watts per $mm^2$ and at $223^{o}K$, $1.2 \times 10^{-9}$ watts per $mm^2$ at the focal plane of the telescope. This means that at the present stage of development, a ferroelectric bolometer such as the#G-20311 can be used, for example, for thermal measurements of the Lunar surface.

## ACKNOWLEDGMENTS

This work was sponsored by the National Aeronautics and Space Administration under Grant No. 64-60.

The authors wish to thank Mr. N. W. Cunningham, former Acting Head, Lunar Sciences, NASA, for his continued encouragement throughout the development program. Acknowledgment is also due to Mr. Daniel Malaise (Astrophysical Institute, Liege, Belgium) for his valuable assistance in some of the measurements, Mr. H. Gerald Gross for his contributions in vacuum tube techniques and Mr. Dieter Fröehling for his general assistance during the course of the experimental work.

# BIBLIOGRAPHY

1. H. C. Ingrao and D. H. Menzel, "Instrumentation for Observations of Planets in the Far Infrared," Memoires Soc. R. Sc. Liege, cinquiemeserie, Tome VII.

2. G. Diemer, G. J. van Gurp and W. Hoogenstraaten, Phillip Res Repts. 13, 458 (1958) and 14, 11 (1959).

3. W. D. Brennan, "Uncooled IR Detector for the Ten Micron Region," Report No. ARF-1208-12A, Feb. 25, 1963 - Armour Research Foundation.

4. Russell DeWard and Eric M. Wormser, "Thermistor Infrared Detectors," Part I NAORD 5495, April 30, 1958.

5. Hector C. Ingrao and D. H. Menzel, "Study of Infrared Instrumentation for Thermal Photography of the Moon," Semiannual Status Report No. 2, NASA Grant NsG 64-60, Harvard University, July to December, 1960.

6. H. C. Ingrao and D. H. Menzel, "Infrared Work at Harvard College Observatory," Informal Infrared Astronomy Symposium, Nov. 11, 1961, Lab of Astrophysics and Physical Meteorology, The Johns Hopkins University, Baltimore, Maryland.

7. Jay Burns, "Thermal Image Tube," Chicago Midway Laboratories, The University of Chicago, June 1956.

8. R. A. Hanel, "Dielectric Bolometer, A New Type of Thermal Radiation Detector," J.O.S.A., 51, 2, 220, 1961.

9. J. Cooper, "Minimum Detectable Power of a Pyroelectric Thermal Receiver," Rev. Sci. Instr., 33, 1, 92, 1962.

10. B. L. Mattes and T. A. Perals, "Transducer for the Measurement of Thermal Power," Rev. Sci. Instr., 32, 3, 332, 1961.

11. S. B. Lang, "Temperature, Its Measurement and Control in Science and Industry," 27-31 March 1961, Fourth Symposium on Temperature, Columbus, Ohio.

12. Boeing Company, "Study of Advanced Solid State Infrared Detection," Final Report Contract No. AF 33(616)-7549 U.S. Air Force, November, 1962.

13. T. A. Perals, T. J. Diesel and W. I. Dobrov, "Primary Pyroelectricity in Barium Titanate Ceramics," J. Appl. Phys. 29, 1297 (1958).

14. R. A. Smith, F. E. Jones and R. P. Chasmar, "The Detection and Measurement of Infra-Red Radiation." Oxford University Press, London, 1957.

15. A. B. Gillespie, "Signal Noise and Resolution in Nuclear Counter Amplifiers." McGraw-Hill Book Co., Inc., New York, 1953.

16. K. R. Spangenberg, "Vacuum Tubes." McGraw-Hill Book Co., Inc., New York 1948.